Scientific Paper / Artículo Científico

UNIVERSIDAD POLITÉCNICA SALESIANA ECUADOR
INGENIUS
Revista de Ciencia y Tecnología
https://doi.org/10.17163/ings.n30.2023.10
pISSN: 1390-650X / eISSN: 1390-860X

Monte Carlo simulation of uncontrolled Electric Vehicle charging impact on distributed generation

Impacto de la Simulación MonteCarlo de Carga no controlada de vehículos eléctricos en la generación distribuida

Villanueva-Machado, Carlos W.[1,*], Jaime E. Luyo[1], Rios-Villacorta, Alberto[2],

Received: 08-05-2023, Received after review: 31-05-2023, Accepted: 12-06-2023, Published: 01-07-2023

Abstract

The uncontrolled charging of electric vehicles poses a great challenge for distribution network operators and power system planners. Instead of focusing on controlling this uncontrolled load, a model that uses contingency analysis variables to calculate the power capacity needed in the power system is proposed. The unserved power variable is used to evaluate the amount of uncovered load power at each bus of the system, followed by the calculation of the additional power capacity required using a photovoltaic and storage system and another constant generation alternative in the 14-bus IEEE power system with information on some electric vehicles and daily load in the power system of Peru. The results obtained in the power system with distributed generation, the absence of unserved power, corroborate the success of the methodology used. This model provides tools to both distribution network operators and power system planners, reducing the impact on the power system of electric vehicles and providing a methodology applicable to other electric distribution systems with uncontrolled loads.

Keywords: Electric Vehicles, Energy Storage Systems, Monte Carlo Simulation, Not Served Power, Optimal Power Flow, Renewable Energy Sources, Power System

Resumen

La carga no controlada de vehículos eléctricos plantea un gran desafío para los operadores de redes de distribución y los planificadores de sistemas de potencia. En lugar de focalizarse en el control de esta carga no controlada, se propone un modelo que utiliza variables de análisis de contingencias para calcular la capacidad de potencia necesaria en el sistema de potencia. Se emplea la variable de potencia no servida para evaluar la cantidad de potencia de carga no cubierta en cada barra del sistema, seguido del cálculo de la capacidad de potencia adicional requerida utilizando un sistema fotovoltaico y de almacenamiento y otra alternativa de generación constante en el sistema de potencia IEEE de 14 barras con información sobre algunos vehículos eléctricos y la carga diaria en el sistema de potencia de perú. Los resultados obtenidos en el sistema de potencia con generación distribuida muestran que no hay presencia de potencia no servida, corroborando el éxito de la metodología utilizada. Este modelo brinda herramientas tanto a los operadores de redes de distribución como a los planificadores de sistemas de potencia, reduciendo el impacto en el sistema de potencia de los vehículos eléctricos y aportando una metodología aplicable a otros sistemas de distribución eléctrica con cargas no controladas.

Palabras clave: Fuentes de Energía Renovable, Potencia no Servida, Sistema de Potencia, Sistemas de Almacenamiento de Energía, Simulación de Monte Carlo, Vehículos Eléctricos

[1,*]Faculty of Mechanical Engineering, Universidad Nacional de Ingeniería, Perú.
Corresponding author ✉: cwvillanuevam@uni.pe.
[2] Faculty of Systems Electronics and Industrial Engineering, Universidad Técnica de Ambato, Ecuador.

Suggested citation: Villanueva-Machado, C. W.; Luyo, J. E. and Rios-Villacorta, A. “Monte Carlo simulation of uncontrolled Electric Vehicle charging impact on distributed generation,” *Ingenius, Revista de Ciencia y Tecnología*, N.° 30, pp. 120-134, 2023, doi: https://doi.org/10.17163/ings.n30.2023.10.

1. Introduction

Electric Vehicles (EVs) have become popular due to their low emissions, high efficiency, and lower operating costs [1]. However, the increase in EVs has created challenges for the electricity grid, including uncontrolled charging that strains distribution networks (DNs). This article proposes a system consisting of photovoltaic (PV) generation and battery energy storage (ES) that can be implemented to optimize the use of PV and battery systems, minimize the cost of EV charging, and reduce grid load [1, 2].

EVs present challenges to power grid capacity, charging infrastructure, and ES technology [3, 4]. Vehicle-to-Grid (V2G) and Distributed Generation (DG) have been proposed as supportive technologies to address these issues [1]. A model of the impact of local EV adoption on DNs is presented in [5], posing a challenge to Distribution Network Operators. Monte Carlo simulation (MCS) can assist operators in understanding the impact of their policies on system performance and identifying potential risks associated with certain decisions [6] as a way to address these issues.

According to a study by [7], MCS usage is a valuable tool for assessing the impact of uncertain factors on the performance of power systems (PSs). The operating condition of the electricity DN can be enhanced using MCS. The presence of the variable Not Served Power (NSP) shows energy-depleted or overloaded PSs operation conditions.

PV generation and ES technologies have been proposed as potential solutions for integrating EVs into the power grid, as suggested in [1], [6]. NSP optimization has been proposed as a method for monitoring PS performance. This method covers operational costs in contingencies, as NSP will be expelled from the load [8]. V2G technology is also a solution to the challenges of uncontrolled EV charging, since it can help mitigate negative aspects and improve sustainability [9]. MCS has been suggested as a potential tool for analyzing the impact of DG supplying surplus load required by EVs.

A description of complementary analysis examines the interaction with the EVs adoption. The interaction between the intermittency generated by renewable generators and the storage capacity allowed using the V2G charging process is described in [2]. A stochastic methodology associated with EVs smart charging process is considered in [4], focusing on battery degradation analysis. While [3] is focused on the interplay between different variables required for a smart charging process. The Internet of Energy environment is adapted according to future smart grid operation required.

As proposed in [10], DG can help mitigate the negative impacts of uncontrolled EV charging and improve sustainability. DG can supply energy to the grid during peak hours and balance the load, reducing the impact of uncontrolled EV charging on the power grid. To determine appropriate energy policies, it is important to anticipate energy deficiencies. Reference [5] proposes a model that characterizes the geographic and travel patterns of EV owners' behavior. This provides insights into their travel behavior and energy demands.

The study proposed MCS usage to analyze the midterm effects of uncontrolled EV charging. This contributes to establishing energy policies that meet the energy demands of EV owners. These measurements' implementation enhanced the stability and reliability of the electricity DN.

The method generates snapshots of potential scenarios based on global trends and Peru's EV transportation market, and it is valuable in optimizing the electricity DN using algebraic modeling. The study aims in developing policies that meet energy demands while ensuring stable and reliable electricity DN conditions. The need for future charging stations and DG strategies due to EV charging is highlighted in [6].

2. Materials and Methods

Different levels of EVs adoption will be analyzed to evaluate the impact on DN energy required, using worldwide and Peruvian information. The projection reviews Peruvian actual and historical vehicle fleet stratification.

The methodology presented in the article involves a loop that starts from EV model information and goes up to the stage of saving data, as illustrated in Figure 1. This loop is applied to all EV models and the three scenarios of EV adoption mentioned in the section "2.3 Multiple Scenarios." Table 1 shows the terminology employed in the current paper.

The resulting data is then processed through 2 separate processes. The MCS is the first process, reducing the amount of data. The DN analysis explained in section "2.8" is the second process. The information gathered from these processes is used to compare and evaluate the designed system that integrates PV generation and ES to tackle the surplus energy demand caused by uncontrolled charging of EVs on the DN.

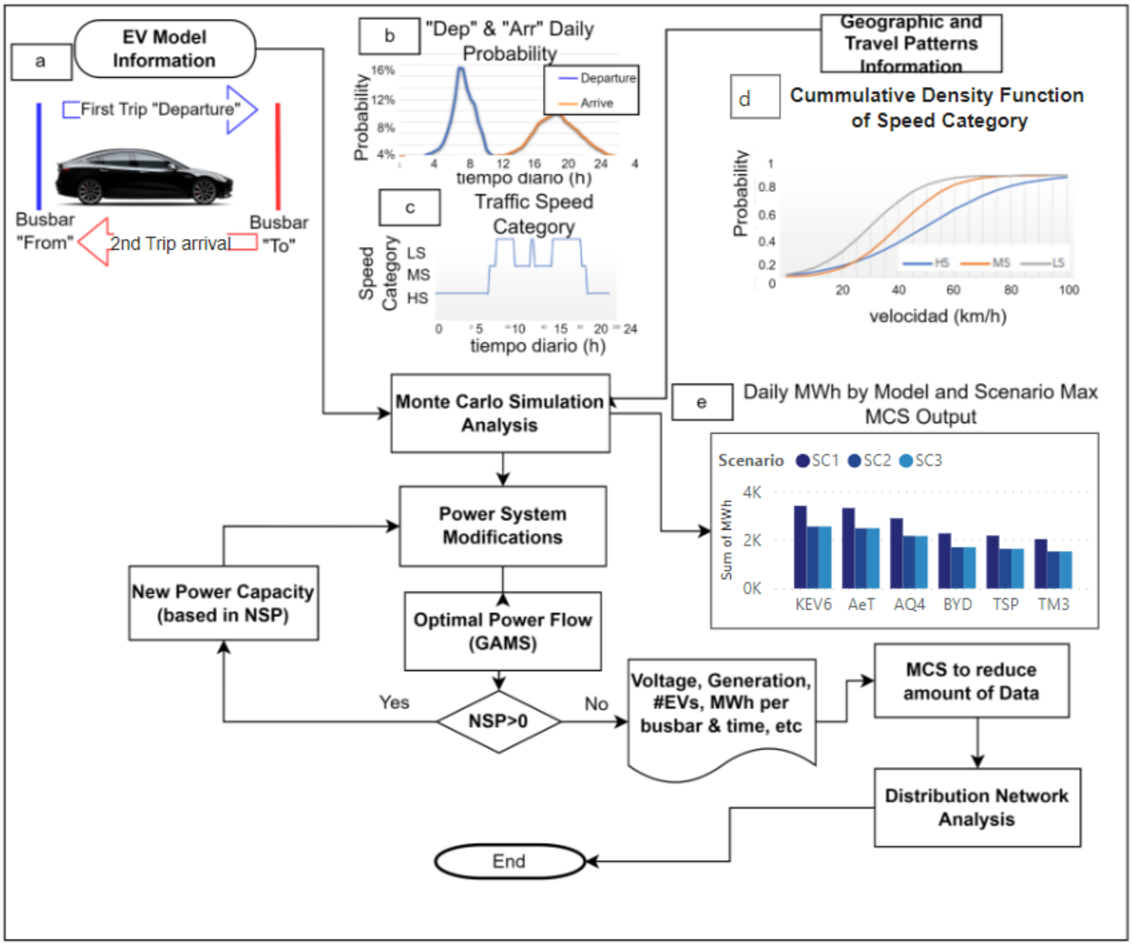

Figure 1. Methodology and input data: (a) Monte Carlo simulation input related to electric vehicle models, and explanations of daily travels (b) daily trip times probability density function (PDF) (c) daily traffic speed category (d) speed value cumulative density function per traffic speed category (e) results from Monte Carlo simulation, input for next steps

Table 1. Terminology employed in the current paper

Terminology	Description
PS	Power System
MCS	Maximum Continuous Service
V2G	Vehicle-to-Grid
GAMS	General Algebraic Modeling System
NSP	Not Served Power
EVs	Electric Vehicles
PC	Power Capacity
DG	Distributed Generation
DN	Distribution Network
PV	Photovoltaic
ES	Energy Storage
OPF	Optimal Power Flow
NSE	Not Served Energy

2.1. Uncontrolled charging projection description in Peru

Peruvian EV imports have been rising (as reported by the Economic Studies Department of AAP, 2019) since 2016. Until August 2019, there were 253 hybrid and 16 electric vehicles imported. The global number of yearly electric vehicles imported was 11 in 2016, 93 in 2017, and 165 in 2018. In total, 535 EVs were reported until August 2019. Peruvian government reported the number of vehicles on the road until 2018 of each category: cars, station wagons, and pickup tracks.

2.2. Uncontrolled charging projection process in Peru

The task projects the optimistic, pessimistic, and business-as-usual electric vehicle (EV) adoption rates in Peru. This estimates the controllable charging rate using market participation as a point of reference and calculating the uncontrollable charging rate. The uncontrollable charging rate is calculated as a complement of the controllable charging rate, which is assumed to vary yearly depending on regional and global EV adoption trends.

The assumptions for the pessimistic and optimistic projections are based on current trends. They may not hold in the future. Electric vehicle sales are expected to continue increasing due to government incentives, reduced battery costs, and increased consumer awareness.

2.3. Multiple scenarios

This study examines the potential impact of EV adoption on energy demand in Peru's PS. Three growth scenarios for EV adoption are presented: low (15% per year), medium (25% per year), and high (40% per year). Three scenarios of 2000, 2500, and 3750 EVs estimate the number of uncontrolled charging EVs in the medium term. The scenarios were developed using Peruvian and worldwide data [11].

Based on the scenarios, the authors evaluated the potential impact of EV adoption on Peru's PS under different conditions. The selection criteria for the scenarios were based on realistic and varied growth rates, worst-case analysis, and historical and current data. A review of Peru's actual and historical vehicle fleet stratification is also provided.

As of August 2019, 253 hybrids and 16 EVs were imported into Peru. The Peruvian government reported the number of vehicles on the road until 2018 for each category [12]. For further details, refer to section 2.2.

2.4. Monte Carlo simulation analysis

Figure 1a shows how EVs depart from and arrive at different busbars, with departure and arrival times based on EV owner travel and geographic patterns [5]. The model uses Ns samples (s), T time periods (t), and $NV\ EVs$ (v) characterized with stochastic variables [13].

Figure 1b displays the stochastic variables [9], $dep_{v,s}$ and $arr_{v,s}$ that are fit into probabilistic distributions [2], with binary variables representing the states ($deps_{t,v,s}$ and $arrs_{t,v,s}$). Figure 1c and 1d depict probability characterizations of EV speed variable ($sv_{t,v,s}$) and distance between buses corrected using $tdcf_{v,s}$ and length $L(Fr_{v,s} : To_{v,s})$.

$$td_{v,s} = L(Fr_{v,s}; To_{v,s}) \times tdcf_{v,s} \tag{1}$$

Equation (1) combines stochastic parameters of EV location state $Fr_{v,s}$ and $To_{v,s}$, with $tdcf_{v,s}$ to determine the final travel distance $td_{v,s}$. Specific EV data is required for MCS analysis, such as Battery Capacity (BCES), Riding Specific Consumption ($SC_{v,s}$), State of Charge (SoC_{min} and SoC_{max}), maximum charging power (Pv_{max}), charging and discharging efficiency (n_{chg} and n_{dsg}), road consumption value ($R_{t,v,s}$), and binary variable index ($X_{t,v,s}$).

2.4.1. Pseudo code – travel modeling

1. Define departure time or arrival time and temporal road distance travelled variable $t = dep_{v,s}$ and on road distance travelled, $rdt_{v,s} = 0$ for departure & $t = arr_{v,s}$) and $rdt_{v,s} = 0$ for arrival travel.

2. Start Loop to fill the road distance traveled until surpassing the travel distance, as in equations (2) and (3).

$$while\ rdt_{v,s} \leq td_{v,s}\{ \tag{2}$$

$$rdt_{v,s} = +sv_{v,s} \times 24/T \tag{3}$$

3. Conditional to check if the last stage of departure travel is reached as in equations (4) and (5).

$$if\ rdt_{v,s} \leq td_{v,s}\{ \tag{4}$$

$$R_{t,v,s} = sv_{v,s} \times SC_{v,s}/n_{dsg} \times 24/T \tag{5}$$

4. Assign a value to on-road consumption for non-last stages of departure travel as in equation (6).

$$else\{R_{t,v,s} = (sv_{v,s} + td_{v,s} - rdt_{v,s}) \times SC_{v,s}/n_{dsg}\} \tag{6}$$

5. End loop assigning the value of departure end time or arrival start time and binary state of on-road as in equation (7)) for departure trip and equation (8) for arriving trip.

$$X_{t,v,s} = 1 \wedge t = +1\} de_{v,s} = t \tag{7}$$

$$X_{t,v,s} = 1 \wedge t = -1\} ai_{v,s} = t \tag{8}$$

Variables such as $de_{v,s}$ and $ai_{v,s}$ mark the end of the departure trip and the time when the EV is ready to begin the return trip, respectively.

The binary variable $CS_{b,t,v,s}$ tracks the charging bus state for the EV allocated in bus b. Equations (9) and (10) enforce constraints related to the charging bus state.

$$CS_{Fr_{v,s},t,v,s} = 1 \forall arr_{v,s} < t < dep_{v,s} \tag{9}$$

$$CS_{To_{v,s},t,v,s} = 1 \forall de_{v,s} < t < ai_{v,s} \tag{10}$$

The variables $ChR_{v,s}$ and CC are defined as the total energy required by the EV on the road and the complete charge, respectively. These variables are assigned in equations (11) and (12), respectively.

$$ChR_{v,s} = \sum_t R_{t,v,s} \tag{11}$$

$$CC = Pv_{max} \times 24/T \times n_{chg} \tag{12}$$

2.4.2. Pseudo code – uncontrolled charging modeling

1. Set 0 value to $tch_{v,s}$ as in equation (13).

$$tch_{v,s} = 0; \forall v \in NV \wedge s \in Ns \tag{13}$$

2. Set charging time: departure and arrival as in equation (14).

$$t = de_{v,s} \wedge t = arr_{v,s} + 1 \tag{14}$$

3. Increase and assign the value of uncontrolled vehicle charge $UC_{b,t,v,s}$, according to temporal charge $tch_{v,s}$, measuring uncontrolled charging in the corresponding bus, without reaching the energy required as in equations (15) and (16).

$$tch_{v,s} = +CC \tag{15}$$

$$if\ tch_{v,s} \leq ChR_{v,s} \{UC_{b,t,v,s} = CS_{b,t,v,s} \times CC\} \tag{16}$$

4. Assign uncontrolled charge to the time while reaching the energy required as in equation (17).

$$else\{UC_{b,t,v,s} = (ChR_{v,s} + CC - tch_{v,s}) \times CS_{b,t,v,s}\} \tag{17}$$

5. End loop as in equation (18).

$$t = +1\} \tag{18}$$

Equation (19) is used to obtain the information on the required Peak Load, PLR_s, which is reported as the final output of the MCS. The load of PS in bus b is represented by $Pdps_{b,t}$. Figure 1e provides a summary of this information, showing the daily cumulative energy required by the DN for all models and scenarios. Figure 1e compares only the maximum MCS outputs, which cause more DN load during peak hours. On the other hand, the minimum MCS output represents the minimum impact on the peak hour charging state.

$$PLR_s = max\left(t, \sum_b \left(\sum_v UC_{b.t.v.s} + Pdps_{b,t}\right)\right) \tag{19}$$

2.5. Interaction between MCS and optimal power flow

Equations (21) and (22) show how the outputs of MCS are chosen. The surplus charge is added to the PS load and denoted as $Pd_{b,t,s}$. The information obtained from MCS analysis (Equations (21) and (22)) is an important input for optimizing the operation of the electricity DN, specifically the transmission subsection, using algebraic modeling.

$$[PLR_{smax}, smax] = max(s, PLR_s) \tag{20}$$

$$[PLR_{smin}, smin] = min(s, PLR_s) \tag{21}$$

$$Pd_{b,t,s} = Pdps_{b,t,s} + \sum UC_{b,t,v,s} \tag{22}$$

2.6. Optimal power flow analysis

The electric OPF is modeled in GAMS software, using CONOPT minimizing of from equation (24) for each of the 6 cases (3 scenarios, 2 MCS outputs). This process provides the amount of NSP required in each bus of the DN for each period analyzed, as in equation (25). GAMS optimization and MCS complementary analysis approaches could overcome the challenges of integrating EVs and DG into PSs [14].

2.6.1. Objective function

The main output is the energy allocated to daily Not Served Energy (NSE) with half-hourly information. It involves evaluating equations for all $t \in T \wedge s \in \{s_{min}, s_{max}\}$. NSE is used to allocate the amount of NSP during this time period, as per equation (23).

NSP is used as a slack variable to identify areas and the amount of energy required for surplus EV charging, and it can also represent the amount of power required as surplus generation in its busbar to avoid PS failures [8].

The objective function (of) for the optimization of energy losses associated with network operation is expressed in equation (24), where the power generation at the slack bus Pg_{slack} is also evaluated. The penalty price of $C_{pen} = \$6,000.00$ for NSE in Peru is mentioned according to reference [15]. Using NSP as a data source can help planners compare generation source alternatives, fit the energy required in time-space modeling, and dimension the DG conditions along the PS.

$$NSE_k = 24/T \times NSP_k \tag{23}$$

$$of = \sum (C_{pen} NSE_k) + Pg_{slack} \tag{24}$$

2.6.2. Optimal power flow constraints

The OPF constraints are the active and reactive power balance. Equations (25) and (26) define the power balance, where Pg_k and NsP_k denote generation power and non-spinning reserves, while Pd_k represents the required power load.

$$Pg_k + NSp_k = Pd_k + \sum P_{km} \quad (25)$$

$$Qg_k = Qd_k + Qsh_k + \sum Q_{km} \quad (26)$$

The variables Qg_k, Qd_k, relate to reactive power generation and load in each bus. Equations (27) and (28) calculate the active and reactive power per line (P_{km} and Q_{km}) and apparent power S_{km} in equation (29) controls the overcharge in the corresponding power line.

$$P_{km} = V_k V_m Y_{km} cos(th_{km} + d_{km}) - V_k^2 cos(t_{km}) \quad (27)$$

$$Q_{km} = -V_k V_m Y_{km} sin(th_{km} + d_{km}) + V_k^2 sin(t_{km}) \quad (28)$$

$$S_{km} = \sqrt{P_{km}^2 + Q_{km}^2} \leq S_{kmupper} \quad (29)$$

The variables V_i, d_i, Qg_i, Pg_i have lower and upper bounds, denoted by x_{lower} and x_{upper} in equation (30). The section refers to [8] for details on voltage parameters (V and d) and admittance matrix parameters (Y and t).

$$x_{lower} \leq x \leq x_{upper} \quad (30)$$

2.7. New power system capacity to guarantee normal operation

Two alternative options were considered for the model developed to determine the failure time and bus. The first option involves a linear increase in Power Capacity (PC) in a specific bus. The second option is a combination of PV generation and an ES system.

Equation (31) describes the first option, which models new PC ($PNg_{k,t}$) to operate throughout the day to recover the investment costs. The second option aims to minimize the objective function of over costs with suffix cost x_{cost} related to NSP calculated ($NSPc_{k,t}$).

$$PNg_{k,t} = Pg_{k,t} + NSPc_{k,t} \quad (31)$$

Equations (32) to (34) describe the process of the second option, which covers the new PC required, including power dimension ($PhPC_b$) and energy storage ($SSEC_b$), and is adjusted to solar availability (Saf_t) and States of Charge variation ($SoCv_{k,t}$) to redistribute energy stored half hourly (Dt). The source of surplus generation capacity is not analyzed due to its variety.

$$fo = PhPC_{cost} \times PhPC_k + SSEC_{cost} \times SSEC_k \quad (32)$$

$$PhPC_k \times Saf_t \geq NSPc_{k,t} + SoCv_{k,t} \quad (33)$$

$$SoC_{k,t} = SoC_{k,t-1} + SoCv_{k,t-1} \times Dt \quad (34)$$

2.8. Distribution network impact

Studies indicate that EVs have an impact on DNs. The daily energy requirements are independent of the EV model. The voltage data and the energy required by EVs are collected and processed through data science, obtaining statistical information using MCS. The EVs charging can cause voltage drops and instability in the network, which can be addressed by using ES systems and smart charging strategies [2], [5].

2.9. Study Case

2.9.1. Uncontrolled charging projection results in Peru

Assumptions and sources of information use market participation as a reference point for regional and global controllable charging rates. The cumulative EV sales are assumed as total on-road EVs, and EV sales are expected to continue increasing due to government incentives, reduced battery costs, and increased consumer awareness.

The optimistic projection assumes a yearly increase in EV sales of 25%, and the controllable charging rate is assumed to be 70%. The pessimistic projection assumes a yearly increase in EV sales of 10%, and the controllable charging rate is assumed to be 50%. These assumptions were used to project EV adoption in Peru.

Table 2 presents ranges of the projection of EV adoption in Peru from 2023 to 2031. This includes cumulative EV sales, controllable and uncontrollable charging rates, and the number of EVs on the road. The data is presented in ranges, from optimistic, pessimistic, and business-as-usual scenarios.

Table 2. Uncontrolled charging electric vehicles (projected data 2023 - 2031)

Year	Total Vehicles N°	Cumulative EV Sales N° EVs	Market Participation %	Uncontrollably Charging Rate %	Uncontrolled Charging EVs N° EVs
2023	366,900-372,700	2,450-2,930	6.67%-7.85%	85.30%-86.70%	2,120-2,490
2024	375,800-385,900	3,180-4,170	8.45%-10.81%	84.30%-85.80%	2,719-3,460
2025	384,000-399,800	4,200-5,750	10.94%-14.39%	83.30%-84.90%	3,606-4,880
2026	392,300-414,500	5,480-7,770	13.97%-18.74%	82.30%-84.00%	4,760-7,070
2027	400,800-430,000	7,190-10,350	17.95%-24.07%	81.30%-83.10%	6,455-9,060
2028	409,400-446,400	9,370-13,500	22.84%-30.21%	80.30%-82.20%	8,485-11,978
2029	418,200-463,700	12,030-17,350	28.73%-37.40%	79.30%-81.30%	10,963-16,652
2030	427,100-482,100	15,220-22,020	35.63%-45.65%	78.30%-80.40%	14,372-17,494
2031	436,100-501,600	18,920-27,650	43.31%-55.31%	77.30%-79.50%	15,390-24,768

2.9.2. Multiple scenarios

The article is based in three scenarios for the growth of EV sales in Peru: optimistic, business-as-usual, and pessimistic, with controllable charging rates estimated for each scenario. Based on this information and analysis of uncontrolled charging of EVs, the study projects that the number of EVs on the road in Peru for 2023 will range from 2450 to 2940. The article also compares the technical characteristics of different EV models and their effects on the DN, as shown in Table 3, with the KIA EV6 found to require the most energy among the EVs studied. However, the scenarios presented are based on broad assumptions and may not accurately reflect the specific conditions of the Peruvian market. More information is shown in Table 2.

Table 3. Electric vehicle models (2,021 data)

EV	BCES kWh	SCv,smin kWh/km	SCv,smax kWh/km	Pvmax kW	SoCmin %	SoCmax %
TSP	100	0.18	0.21	250	5	80
AQ4	82	0.181	0.181	125	15	95
KEV6	77.4	0.21	0.227	228	10	80
BHEV	76.9	0.164	0.207	360	30	80

2.9.3. Monte Carlo simulation analysis

The study analyzed three scenarios with stochastic micro scenarios. Scenario 1 had 2,000 EVs with 200 samples. Scenario 2 had 2,500 EVs with 120 samples. Scenario three 3 had 3,750 EVs with 80 samples. The analysis included $1.0 \times 10^{+6}$ uncertainty stochastic micro scenarios. In Section 2.4, the variables $dep_{v,s}$ and $arr_{v,s}$ were fitted to a normal distribution. Figure 1b illustrates significant differences between the probability distribution functions of departure and arrival times. The arrival time has a standard deviation encompassing after-work hours when individuals may attend to household duties or socialize after work, which does not occur similarly during morning hours before work.

According to [13], the Tesla Model 3 has a $BCES$ of $2.88{\times}10^{+8}$ J (80 kWh). The specific energy consumption for the vehicle falls within the range of $SC_{v,s} \in < 684; 900 > J/m (< 0.19; 0.25 > KWh/Km)$. The EVs maximum charging power is approximately $Pv_{max} = 1.5 \times 10^{+5}\ W$ with $n_{chg} = 90\%$ and $n_{dsg} = 90\%$. To model EV batteries, the minimum State of Charge SoC_{min} is set to 15% of the battery capacity, while the maximum State of Charge SoC_{max} is set to 95% of battery capacity.

2.9.4. Interaction between MCS and OPF

Travel and geographic uncertainties characterization involves categorizing the number of EVs per bus as either "From" or "To" bus based on the departure trip. Figure 2 displays boxplots of the hourly total energy required by the DN, comparing the KIA EV6, which requires the greatest amount of energy, with the Tesla Model 3, which requires the least energy (as seen in Figure 1e). The values reported in Figure 2 show that the KIA EV6 is the model that consumes more energy, triggering a higher energy requirement for the DN.

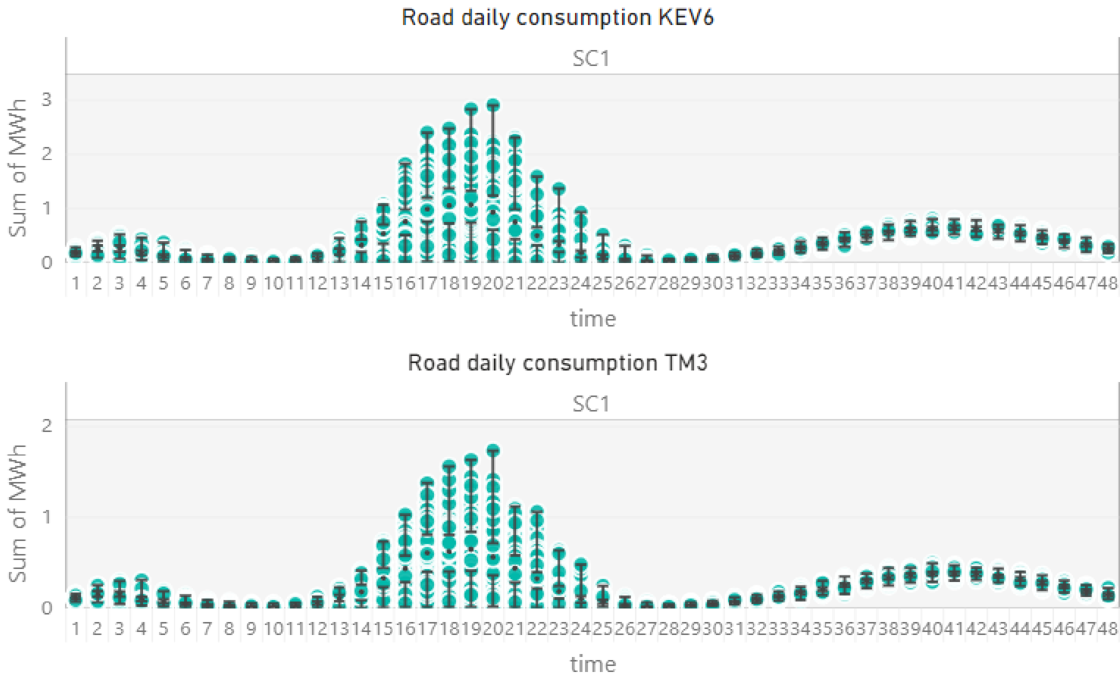

Figure 2. Road daily consumption needed per scenario and time

2.9.5. Optimal power flow usage

The IEEE 14 Power Bus System [16] represents the PS of socioeconomic class A in Peru with variations in power line length. The electric market load data from February 2020 serves as the daily load factor. The traffic categories effects of high, medium, and low speed are reported on [13]. Google Maps provided traffic history data for three categories represented by normal distributions. The first category is high speed, with a mean value of 13.89 m/s (50 km/h) and a standard deviation of 5.56 m/s (20 km/h). The second category is medium speed, with a mean value of 9.72 m/s (35 km/h) and a standard deviation of 4.17 m/s (15 km/h). The third category is low speed, with a mean value of 5.56 m/s (20 km/h) and a standard deviation of 2.78 m/s (10 km/h).

2.9.6. New power system capacity to guarantee normal operation

The first surplus PC option needs no additional data, but the PV generation with storage system option requires a solar availability factor, obtained from [17], with cost data from [18]. Subsection 2.7 presents constraints and the objective function of power interaction with NSP. Constraints (32) to (34) are complemented by equation (35), limiting the $SoC_{k,t}$ variable to the bounds of 0 and the capacity of the storage system, $SSEC_k$.

$$0 \leq SoC_{k,t} \leq SSEC_k \tag{35}$$

The objective function variables in equation (33) include $PhPC_{cost}$ at 1.30 \$/W for photovoltaic PC cost and $SSEC_{cost}$ at 1.11×10^{-4} \$/J (400 \$/kWh) for storage system energy capacity.

2.9.7. Distribution network analysis

Two final syntheses that closely resemble the global data are obtained. The first one represented 4% of the occurrences. The other one collected 10% of the occurrences. These reductions are evaluated in a commonly used DN (IEEE 13 BUS power system) using Simulink from MATLAB software. The effect of all the simulations performed on the DN is reported in this section.

3. Results and discussion

3.1. Monte Carlo simulation analysis

Figure 3 shows the number of EVs in the PS and two figures for each scenario, illustrating the geographic and travel patterns of the EVs. Table 4 provides additional information on the number of EVs departing from and arriving at each bus on their first trip, along with geographic patterns uncertainty. The headers in Table 4 are classified as "Min MCS" and "Max MCS," representing the minimum and maximum scenarios of daily peak load reported from MCS outputs. These classifiers can help assess the potential impacts of EVs on the PS.

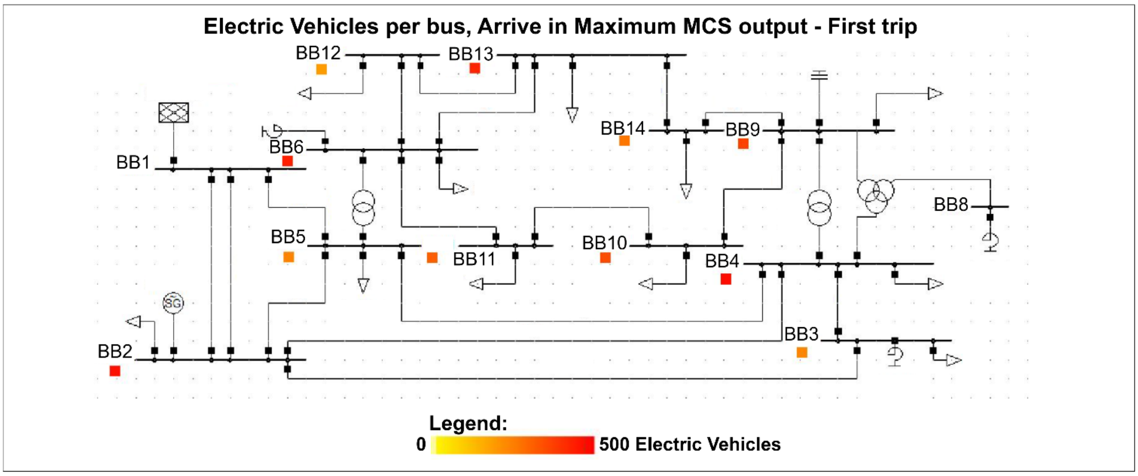

Figure 3. Amount of arriving electric vehicle in maximum Monte Carlo simulation output - scenario 1

Table 4. Number of electric vehicles from and to each bus per scenario for Monte Carlo simulation outputs

	Scenario 1				Scenario 2				Scenario 3			
EVs	**Min MCS**		**Max MCS**		**Min MCS**		**Max MCS**		**Min MCS**		**Max MCS**	
Bus	**Fr**	**To**	**Fr**	**To**	**Fr**	**To**	**Fr**	**To**	**Fr**	**To**	**Fr**	**To**
1	0	0	0	0	0	0	0	0	0	0	0	0
2	180	242	171	269	227	265	224	288	325	460	307	424
3	186	132	197	117	208	151	240	149	337	219	333	227
4	179	255	177	256	215	296	223	336	360	454	342	502
5	204	120	200	103	214	152	227	141	328	217	380	209
6	186	225	188	222	208	339	232	286	320	463	352	440
7	0	0	0	0	0	0	0	0	0	0	0	0
8	0	0	0	0	0	0	0	0	0	0	0	0
9	191	179	166	188	229	256	224	264	358	341	360	342
10	172	196	204	157	244	227	257	242	340	353	322	344
11	172	131	153	164	240	183	232	197	343	287	329	274
12	188	132	201	119	234	150	234	147	357	202	341	221
13	170	244	167	260	249	290	196	280	324	467	337	468
14	172	144	176	145	232	191	211	170	358	287	347	299

3.2. Interaction between MCS and OPF

Figure 4 compares the application for the Tesla Model 3, which has the lowest specific consumption. The first application is the PS_{MCS} which is in the right section. The values are also related to the Maximum output of MCS. Meanwhile, Table 5 presents the mean characteristics of daily load for different scenarios with minimum and maximum MCS outputs.

The energy load Ed_s is computed using equation (36). The peak load $Pd_{max,s}$ represents the maximum daily load supplied by the PS grid for each scenario analyzed, as expressed in equation (37). Finally, the load factor LF_s is determined by dividing the mean power load by the max power load, as shown in equation (38).

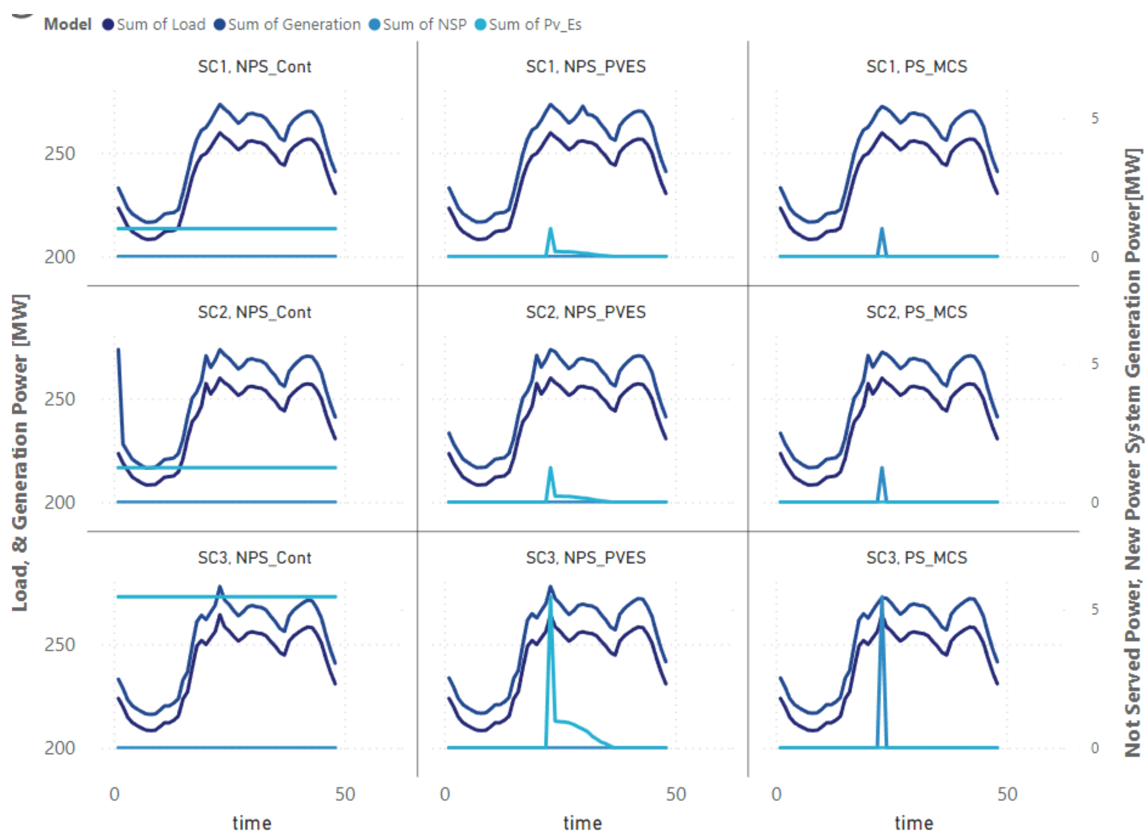

Figure 4. Power System Performance Comparison of Optimal Power Flow (PS_MCS), Photovoltaic and Energy Storage (NPS_PVES), and Continuous Generation (NPS_Cont)

Table 5. Load data per scenarios for Tesla (2018) electric vehicle & Optimal Power Flow performance for all scenarios

Daily Load	BAU w/o EVs	Scenario 1 Min MCS	Scenario 1 Max MCS	Scenario 2 Min MCS	Scenario 2 Max MCS	Scenario 3 Min MCS	Scenario 3 Max MCS
Ed_s (MWh)	5,704.6	5710.58	5724.82	5711.51	5729.43	5715.56	5742.4
$Pd_{max,s}$ (MW)	257.2	257.25	259.66	257.31	259.91	257.51	264.23
LF_s	0.906	0.906	0.907	0.905	0.906	0.910	0.906
Eg_s (MWh)	5,979.1	5985.82	6000.95	5986.67	6005.91	5991.1	6017.9
Los_s (MWh)	274.5	275.24	276.12	275.17	276.48	275.54	275.5
NSE (MWh)			0.5		0.62		2.74
Max NSP (MW)			1.01		1.25		5.47
NSP bus			14		14		14

$$Ed_s = \sum\sum Pd_{b,t,s} \times 24/T; s = \{s_{min}, s_{max}\} \quad (36)$$

$$Pd_{max,s} = max\left(\sum Pd_{b,t,s}\right); s = \{s_{min}, s_{max}\} \quad (37)$$

$$LF_s = \frac{\sum \frac{\sum Pd_{p,t,s}}{T}}{Pd_{max,s}}; s = \{s_{min}, s_{max}\} \quad (38)$$

The difference in peak load between the maximum and minimum MCS outputs was observed to be increasing, indicating the stochastic effect of the analysis. For Scenario 1, the gap between MCS outputs is $2.41 \times 10^{+6}\ W$. For Scenario 2, the difference in MCS outputs is $2.60 \times 10^{+6}\ W$. For Scenario 3, the gap between MCS outputs is $6.72 \times 10^{+6}\ W$. The difference in daily energy load between maximum and minimum MCS outputs is reported per scenario. Scenario 1 has a difference in daily energy of $5.13 \times 10^{+10}\ J$ (14.24 MWh). Scenario 2 has a difference in daily energy of $6.45 \times 10^{+10}\ J$ (17.92 MWh). Scenario 3 has a difference in daily energy of $9.66 \times 10^{+10}\ J$ (26.84 MWh). The increment in the gap is explained due to the number of EVs in the tested scenarios.

3.3. Optimal power flow usage

The model commonly employs OPF to evaluate PS performance concerning different EV charging scenarios. Figure 4 displays the performance of PS and NSP required to maintain normal operation, with the highest output of the Tesla Model 3 EV's MCS specified. Table 5 summarizes the optimized power flow findings, including variables such as Eg_s and $Loss_s$ representing energy generated, energy gaps, and NSE_s allocating NSP for all buses during the day. Equations (39) to (41) define these variables.

$$Eg_s = \frac{\sum\sum Pg_{b,t,s} \times 24}{T}; s = \{s_{min}, s_{max}\} \quad (39)$$

$$Loss_S = Eg_s - Ed_s; s \in \{s_{min}, s_{max}\} \quad (40)$$

$$NSE_s = \frac{\sum\sum NSP_{b,t,s} \times 24}{T}; s = \{s_{min}, s_{max}\} \quad (41)$$

The tested model enables the identification of the bus bar that requires more capacity and whose option is best suited to supply it. The amount of NSP will determine the required capacity for new power plants. Table 6 reports the information for the Tesla Model 3 (2018).

The study found that the NSE was expelled at the last bus of the PS, which is located farthest from the generation buses (#14). The amount of NSE increased as the number of EVs in each scenario.

Table 6. New power system (NPS) capacity to guarantee normal operation as all day fixed value; with photovoltaic - storage system (PSS) option

OPF		**Scenario 1**			**Scenario 2**			**Scenario 3**	
	BAU w/o EVs	**Min MCS**	**Max MCS**	**BAU w/o EVs**	**Min MCS**	**Max MCS**	**BAU w/o EVs**	**Min MCS**	**Max MCS**
Eg_{NPS} (MWh)	5975.91	5982.49	5998.33	5975.16	5982.75	6002.67	5962.67	5974.66	6004.41
$Loss_{NPS}$ (MWh)	271.36	271.91	273.51	270.62	271.25	273.25	258.12	259.1	262.01
Max Pg_{NPS} (MW)	270.7	270.72	273.41	270.67	270.75	273.65	270.08	270.38	277.87
NPS Capacity (MW)		1.01			1.25			5.47	
Eg_{PSS} (MWh)	5978.9	5985.49	6001.34	5978.86	5986.45	6007.05	5978.13	5990.15	6020.07
$Loss_{PSS}$ (MWh)	274.36	274.91	276.52	274.31	274.95	277.63	273.58	274.59	277.67
Max Pg_{PSS} (MW)	270.82	270.83	273.41	270.82	270.84	273.65	270.71	270.72	277.87
PV Capacity (MW)		0.177687			0.219993			0.965943	
Storage System (MWh)		0.419278			0.519105			2.279288	
Busbar (#)		14			14			14	
PSS cost ($)		345,397.68			427,634.56			1,877,658.44	

3.4. New power system capacity to guarantee normal operation

The PS requires additional generation capacity to address the identified problem. The methodology section offers options for obtaining extra generation capacity using: microturbines, internal combustion engines, PV generation mixed with a storage system, etc. Figure 4 displays the performance of the PS and the power supplied by the PV-storage system in Maximum MCS output for the Tesla Model 3. Table 5 provides information about the required capacity of the new power system (NPS). The cost of the PV-storage system is reported for each scenario in Figures 5a, 5b, and 5c, ranging from \$ 0 to \$7.40 $\times 10^{+5}$ for Scenario 1, \$ 2.22 $\times 10^{+5}$ to \$ 7.81 $\times 10^{+5}$ for Scenario 2 and \$ 5.88 $\times 10^{+5}$ to \$3.41 $\times 10^{+6}$ for Scenario 3. The cost of the first option of adding capacity for an entire day is not assessed in this study, but its PC is set constant as NSP from PS OPF.

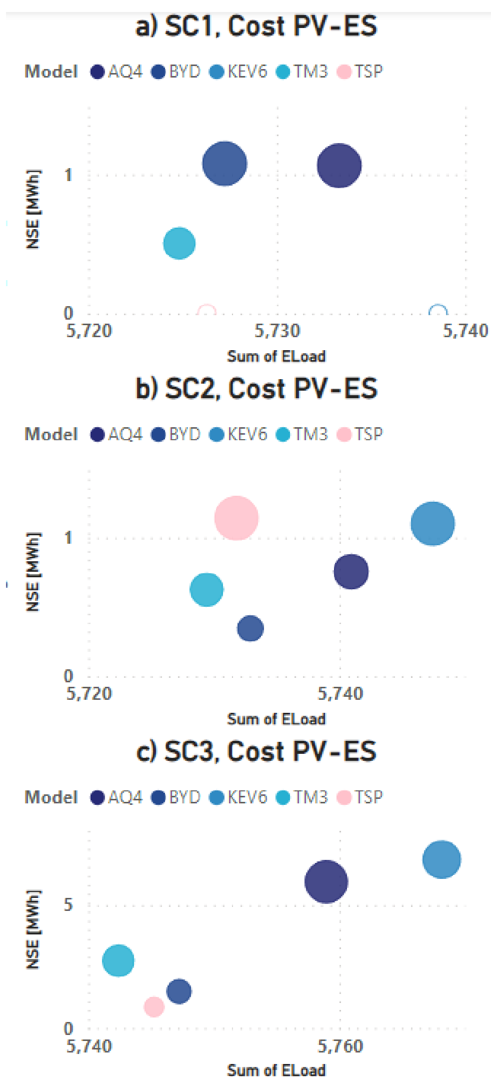

Figure 5. Not Served Energy Comparison and Photovoltaic-Energy Storage Costs for Three Scenarios: (a) for Scenario 1, (b) for Scenario 2 and (c) for Scenario 3

3.5. Distribution network results

Section 3.4 of the study examines the relationship between load and PS capacity. However, increasing the general load does not necessarily require more PS capacity or increase the cost of PV and ES. The study also shows that the load required by EV models does not result in more NSP. These findings suggest that the PS requirements and the EV model are independent.

Data reduction techniques are used to synthesize the large amount of information processed. Two reductions are performed on the data, with errors of 1.24% and 0.85% compared to the global data. The reduction of 4% of the data is used to process the data in MATLAB using the Simulink tool. The DN data is used to redistribute EVs into the feeders of the IEEE 13 bus Power System, and the resulting performance of the feeders is shown in Figure 6. The results indicate that the voltage values remain within range for all buses of the IEEE 13 bus Power System even under uncontrolled charging assumptions.

4. Conclusions

The effect of EVs' uncontrolled charging presence in electricity markets is shown in this study, as seen in Table 5 and Figure 2. The minimum and maximum outputs from the Monte Carlo Simulations depend on the specific consumption of the EV models, which values are reported in Table 3. The EV model that required more energy from the DN is the Kia EV6, while the EV model that required less energy from the DN is the Tesla Model 3, as shown in Figure 1 (e). The highest consumption of scenario 3 is for the Kia EV6 model with 31.8 MWh, while the lowest consumption of scenario 1 is for the Tesla Model 3 with 10.14 MW.

Even for the specific models of EVs that require more energy, the NSP variable is not guaranteed to be needed. Figure 5a shows that the models that did no't have NSP are the Kia EV6 (which has the highest energy need) and Tesla S Plaid. Figure 5b and Figure 5c also reinforce this fact due to the intermittency of maximum and minimum NSP presented in the OPF executions.

On the other hand, the dependency noted in Figure 5 is the relationship between the costs of different dimensions of the PV generation – ES System and the amount of daily NSE presence in the OPF execution. This relationship is not strictly linear, but for similar NSE values, the cost of the system designed is close. For example, in scenario 3, the highest value of NSE is 6.84 MWh. The corresponding EV model is the Kia EV6. The cost related to this point is \$ 2.84 $\times 10^{+6}$. But the highest system designed cost is \$ 3.41 $\times 10^{+6}$ with a not served energy value of 5.94 MWh.

The impact of the uncontrolled charging is not relevant in distribution, as shown by the voltage stability of the executed model. Even the further busbars have voltage values that achieve the Peruvian electric distribution policies' bounds. The busbars 632, 645,646, and 633 have well-distributed voltage levels. The others also have values according to policies.

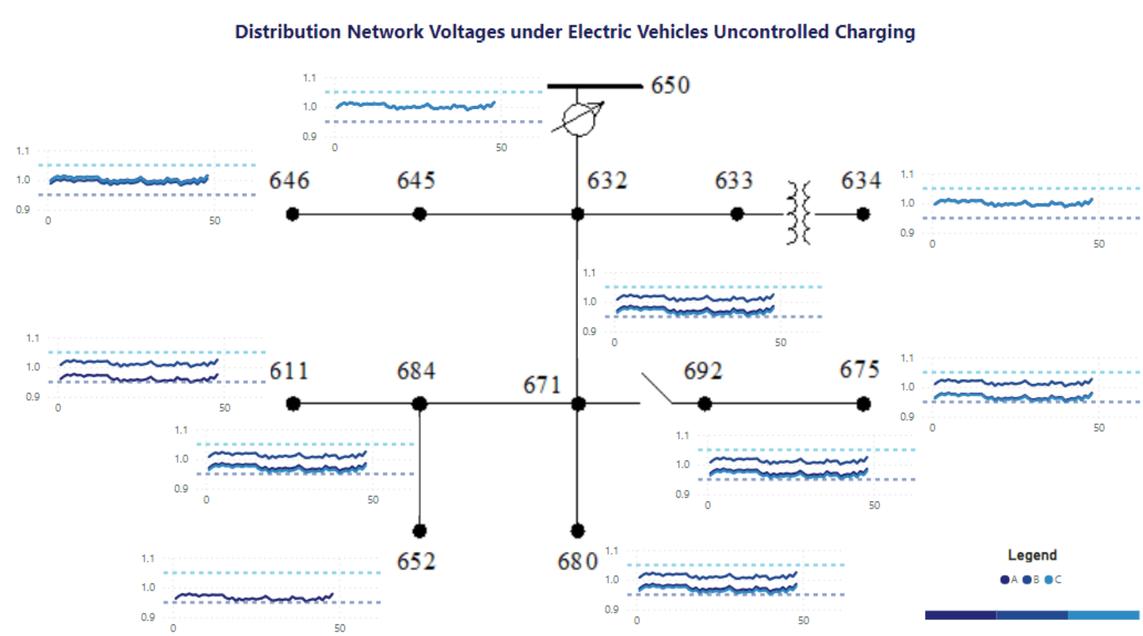

Figure 6. Distribution Network Daily Voltage for each phase

Acknowledgments

A special thanks to the "Program of Doctorates in Peruvian Universities," promoted by the National Council of Science, Technology and Technological Innovation (CONCYTEC) through the National Fund for Scientific, Technological and Technological Innovation Development (FONDECYT).

References

[1] V. Vita and P. Koumides, "Electric vehicles and distribution networks: Analysis on vehicle to grid and renewable energy sources integration," in *2019 11th Electrical Engineering Faculty Conference (BulEF)*, 2019, pp. 1–4. [Online]. Available: https://doi.org/10.1109/BulEF48056.2019.9030787

[2] L. Wang, S. Sharkh, and A. Chipperfield, "Optimal decentralized coordination of electric vehicles and renewable generators in a distribution network using a search," *International Journal of Electrical Power & Energy Systems*, vol. 98, pp. 474–487, 2018. [Online]. Available: https://doi.org/10.1016/j.ijepes.2017.11.036

[3] K. Mahmud, G. E. Town, S. Morsalin, and M. Hossain, "Integration of electric vehicles and management in the internet of energy," *Renewable and Sustainable Energy Reviews*, vol. 82, pp. 4179–4203, 2018. [Online]. Available: https://doi.org/10.1016/j.rser.2017.11.004

[4] A. Ahmadian, M. Sedghi, B. Mohammadi-ivatloo, A. Elkamel, M. Aliakbar Golkar, and M. Fowler, "Cost-benefit analysis of v2g implementation in distribution networks considering pevs battery degradation," *IEEE Transactions on Sustainable Energy*, vol. 9, no. 2, pp. 961–970, 2018. [Online]. Available: https://doi.org/10.1109/TSTE.2017.2768437

[5] R. R. Desai, R. B. Chen, and W. Armington, "A pattern analysis of daily electric vehicle charging profiles: Operational efficiency and environmental impacts," *Journal of Advanced Transportation*, vol. 2018, p. 6930932, Jan 2018. [Online]. Available: https://doi.org/10.1155/2018/6930932

[6] J. H. Angelim and C. de Mattos Affonso, "Probabilistic assessment of voltage quality on solar-powered electric vehicle charging station," *Electric Power Systems Research*, vol. 189, p. 106655, 2020. [Online]. Available: https://doi.org/10.1016/j.epsr.2020.106655

[7] S. Kumar, R. Saket, D. K. Dheer, J. B. Holm-Nielsen, and P. Sanjeevikumar, "Reli-

ability enhancement of electrical power system including impacts of renewable energy sources: a comprehensive review," *IET Generation, Transmission & Distribution*, vol. 14, no. 10, pp. 1799–1815, 2020. [Online]. Available: https://doi.org/10.1049/iet-gtd.2019.1402

[8] C. W. Villanueva Machado, M. F. Bedriñana Aronés, and J. E. Luyo Kuong, *Planificación de expansión de transmisión bajo condiciones de máxima generación con recursos energéticos renovables.* Universidad Nacional de Ingeniería, 2018. [Online]. Available: https://bit.ly/3XfQZ8b

[9] S. Pirouzi, J. Aghaei, T. Niknam, H. Farahmand, and M. Korpås, "Exploring prospective benefits of electric vehicles for optimal energy conditioning in distribution networks," *Energy*, vol. 157, pp. 679–689, 2018. [Online]. Available: https://doi.org/10.1016/j.energy.2018.05.195

[10] S. Lazarou, V. Vita, C. Christodoulou, and L. Ekonomou, "Calculating operational patterns for electric vehicle charging on a real distribution network based on renewables' production," *Energies*, vol. 11, no. 9, 2018. [Online]. Available: https://doi.org/10.3390/en11092400

[11] D. Schmerler Vainstein, J. C. Velarde Sacio, and B. Rodríguez González, Abel Solís Sosa, *Electromovilidad. Conceptos, políticas y lecciones aprendidas para el Perú.* Osinergmin, 2019. [Online]. Available: https://bit.ly/3NBY53W

[12] AAP, *Los Protagonistas de la nueva era automotriz: Vehículos eléctricos e híbridos en el Perú.* Asociación Automotríz del Per"u, 2019. [Online]. Available: https://bit.ly/465w2kl

[13] C. Villanueva, J. Luyo, and C. Delgado, A. Carbajal, "Electric vehicle aggregator participation in energy markets considering uncertainty travel patterns," *International Journal of Innovative Technology and Exploring Engineering (IJITEE)*, vol. 8, no. 12, pp. 4994–4998, 2019. [Online]. Available: https://doi.org/10.35940/ijitee.L3747.1081219

[14] R. Jing, M. Wang, Z. Zhang, X. Wang, N. Li, N. Shah, and Y. Zhao, "Distributed or centralized? designing district-level urban energy systems by a hierarchical approach considering demand uncertainties," *Applied Energy*, vol. 252, p. 113424, 2019. [Online]. Available: https://doi.org/10.1016/j.apenergy.2019.113424

[15] A. Dammert, R. García Carpio, and F. Molinelli, *Regulación y Supervisión del Sector Eléctrico.* Fondo Editorial Pontificia Universidad Católica del Perú, 2013. [Online]. Available: https://bit.ly/3p7rIQW

[16] PSCAD, *IEEE 14 Bus System.* Manitoba HVDC Research Centre, 2014. [Online]. Available: https://bit.ly/3CxmAZt

[17] T. Khatib and W. Elmenreich, "A model for hourly solar radiation data generation from daily solar radiation data using a generalized regression artificial neural network," *International Journal of Photoenergy*, vol. 2015, p. 968024, Oct 2015. [Online]. Available: https://doi.org/10.1155/2015/968024

[18] A. Babajide and M. C. Brito, "Solar pv systems to eliminate or reduce the use of diesel generators at no additional cost: A case study of lagos, nigeria," *Renewable Energy*, vol. 172, pp. 209–218, 2021. [Online]. Available: https://doi.org/10.1016/j.renene.2021.02.088